Development of a Wave-Current Numerical Model using Stokes 2nd Order Theory

Catherine Lloyd[#1], Tim O'Doherty[#2], Allan Mason-Jones[#3]

[#] *School of Engineering, Cardiff University*
Queen's Buildings, 14-17 The Parade, Cardiff, CF24 3AA, UK
[1]Lloydc11@cardiff.ac.uk
[2]Odoherty@cardiff.ac.uk
[3]Mason-JonesA@cardiff.ac.uk

***Abstract* - The optimisation of a Numerical Wave Tank is proposed to accurately model regular waves superimposed on a uniform current velocity. ANSYS CFX 18.0 was used to develop a homogenous multiphase model with volume fractions to define the different phase regions. By applying CFX Expression Language at the inlet of the model, Stokes 2nd Order Theory was used to define the upstream wave characteristics. Horizontal and vertical velocity components, as well as surface elevation of the numerical model were compared against theoretical and experimental wave data for 3 different wave characteristics in 2 different depth tanks. The comparison highlighted the numerical homogeneity between the theoretical and experimental data. Therefore, this study has shown that the modelling procedure used can accurately replicate ocean wave-current conditions providing a potential substitute to experimental flume or tank testing.**

***Keywords* - ANSYS CFX, Computational Fluid Dynamics, Numerical Wave Tank, Regular Waves, Stokes 2nd Order Theory.**

NOMENCLATURE

Symbol	Description
$-C$	Momentum source coefficient (kg/m^3/s)
C_a	Apparent wave celerity, stationary reference frame (m/s)
C_r	Relative wave celerity, moving reference frame (m/s)
H	Wave Height (m)
L	Wavelength (m)
S_z	Source term in z-direction (kg/m^2/s^2)
T_a	Apparent wave period, stationary ref. frame (s)
T_r	Relative wave period, moving ref. frame (s)
U_z	Measured velocity at a certain point (m/s)
$U_{z,spec}$	Target fluid velocity (m/s)
V	Overall volume (m^3)
V_x	Volume occupied by fluid x (m^3)
$\bar{W}$	Mean horizontal velocity (m/s)
a	Wave amplitude (m)
g	Gravitational acceleration (m/s^2)
h	Water depth (m)
k	Wave number (rad/m)
r_x	Volume fraction of fluid x
t	Time (s)
v_a	Vertical velocity component under a wave (m/s)
w_a	Horizontal velocity component under a wave (m/s)
y	Vertical coordinate from the still water level (m)
z	Horizontal coordinate in stream wise direction (m)
η	Surface elevation from the still water level (m)
ω_a	Apparent angular velocity, stationary ref. frame (rad/s)
ω_r	Relative angular velocity, moving ref. frame (rad/s)

I. INTRODUCTION

World energy consumption is predicted to increase by 28% from 2015 to 2040 [1]. This increasing demand for energy coupled with environmental concerns, such as increasing Green House Gas (GHG) emissions, has sparked an interest into sources of renewable energy. Extracting energy from the marine environment has gathered interest over the last decade, with tidal energy being the most promising. It is predicted by [2], that deployment of 3.4 TW of wave and tidal energy capacity could be present by 2050, with 100 GW, equating to around 350 TWh / year, present in Europe.

The development of wave energy devices is very diverse and remains a relatively young industry. The biggest problem is the complex and diverse environment involved in wave energy extraction. Tidal energy, on the other hand, is progressing ahead of wave energy with current developments in tidal range and tidal stream proving very successful. More established projects such as EDF's tidal barrage project, in Brittany (France), has been in operation since 1966 with a capacity of 240 MW producing around 500 GWh / year [3]. More recently, Swansea Bay tidal lagoon (Wales) will be the first of its type using a ring shaped breakwater to impound water instead of spanning a river estuary. The 320 MW prototype will lead the way with larger projects preparing to follow [4]. The MeyGen project (Pentland Firth, Scotland), coordinated by Atlantis Resources [5], is currently the largest planned tidal stream project in the world with a total lease capacity of 398 MW. According to [2], 6 MW of Tidal Stream Turbine (TST) capacity completed installation at the end of 2016 with a further 79.5 MW being undertaken in 2017-19. EDF have also installed 2 x 0.5 MW TST's in 2016, located in Paimpol-Brehat (France). Following this project, EDF are hoping to deploy 7 x 2 MW turbines in Raz-Blanchard (Normandy) in 2018 [6].

These examples alone show the increasing presence that marine energy is having in Europe. However, the high costs associated with the design and deployment of full-scale devices is delaying progress in making these technologies commercially viable and competitive. Complementary to full scale testing, experimental tow tank and recirculating flume facilities are used to test small-scale tidal devices. Experimental testing in tow tank facilities was carried out by [7]–[10] to investigate the influence of surface gravity waves on the performance characteristics of a TST. Wave conditions with varying wave period and height were investigated at different tow speeds. All studies agreed that the average performance of the turbine with waves showed little difference to that without waves. However, values for instantaneous torque and thrust showed substantial oscillations due to fluctuations in the flow induced by the surface gravity waves. A significant loading variation of up to 37% in thrust and 35% in torque measurements were observed by [11]. It was also noted that a recirculating water channel with wave-making facilities would be more representative for investigating wave-current interaction as there is no Doppler shift in the waves of a tow tank. Experimental testing on TST's using recirculating flume facilities were carried out by [12] and found that the turbulence intensity (TI) level of the flow could reach up to 30% upon wave generation.

Small-scale testing could provide invaluable information used in making design considerations, however, designing and testing model-scale devices can also be costly. The need to find a less expensive method to predict TST performance is therefore crucial. One methodology is in the use of Computational Fluid Dynamics (CFD) models. There are many challenges to this approach however, as the marine environment possesses very complex and diverse flow conditions. These flows must be simulated accurately to be able to investigate their effect on submerged marine devices. Such flows arise from interactions between tidal currents, surface waves and turbulence from the bathymetry of the seabed. Faster flow velocities are found near the surface of the water with 75% of the available energy being in the upper 50% of the water depth [13]. More energy can therefore be extracted from near the surface of the water, however, this is where the oscillatory effects produced by waves also have the greatest effect. Waves induce orbital motions which add a horizontal and vertical component to the existing current flow, penetrating the water column by up to half their wavelength [14]. As stated by [7], a compromise must be made between placing a device near the free water surface with the highest velocities, and minimising variations in the horizontal and vertical velocity introduced by surface gravity waves.

A Numerical Wave Tank (NWT) is a numerical representation of an experimental testing facility and can be used to simulate wave-current interactions using various modelling techniques. ANSYS FLUENT 14.5 was used by [15]–[17] to numerically model various wave-current conditions. Irregular waves generated by a piston-type wave maker were modelled by [15], numerically generated combined waves and current conditions were modelled by [16], and [17] modelled regular wave-only conditions which were also generated numerically. All models were validated using experimental data while also comparing against relevant wave theories.

ANSYS CFX 11.0 was used by [18] to model linear water waves generated by a flap type wave-maker and validated against flap type Wave-Maker Theory (WMT). The impact that surface waves have on the performance of a TST was investigated by [19]. This study showed the strength of the oscillatory effects of the wave as well as wave depth penetration through the water depth. Whilst it is crucial that the wave is represented correctly upstream, it is important that feedback from wave reflection is considered.

A method for optimising a NWT model dimensions, mesh, time step and damping technique to prevent wave reflection from the end of the model was presented by [20]. ANSYS CFX 12.1 was used and both linear deep water and finite depth waves were modelled and validated against Linear Wave Theory (LWT) and WMT. It was noted in [20] that an ANSYS academic teaching license was used, this restricts the overall dimensions of the fluid domain and therefore the computational capacity and potentially the accuracy.

This study aims to build upon the findings of previous studies, mentioned above, but for the specific use of ANSYS CFX software. The aim of this work was to establish a working NWT model focusing on accurately simulating wave-current interaction with a uniform current velocity using Stokes 2nd Order Theory (S2OT). In future work the NWT will be used to assess the impact of these loadings on a TST. Without the TST, 3 different wave cases were modelled in 2 different depth tanks, superimposed on a uniform current velocity. Comparisons were made to theory as well as using experimental data obtained by the University of Liverpool to validate the numerical model developed in this study [21].

II. WAVE THEORY

LWT was developed by Airy in 1845 [22] and provides a reasonable description of wave motion in all water depths. LWT relies on the assumption that the wave amplitude is small in comparison to the wave length and therefore higher order terms are ignored allowing the free surface boundary condition to be linearised. If the amplitude is large then the higher order terms must be retained to get an accurate representation of wave motion [23]. These higher order theories were first developed by Stokes in 1847 [24].

The numerical model developed in this study uses Finite Amplitude theory, in particular S2OT, to model regular waves superimposed on a uniform current. S2OT is essentially LWT but with the 2nd order terms included. The coordinate frame is set up so that the z-axis is positive in the stream-wise direction, y-axis is in the vertical direction with 0 at the Still Water Level (SWL) and x-axis is perpendicular to the YZ plane as shown in Figure 1.

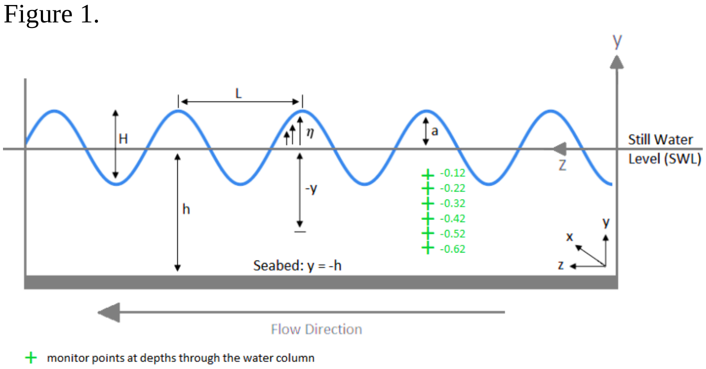

Figure 1. Definition of wave motion.

The relative depth (h/L) and wave steepness (H/L) are 2 of the main parameters that dictate the behaviour of the wave. TABLE I gives the relative depth bounds for deep, intermediate and shallow water waves [21], while TABLE II gives the appropriate theories for various wave steepness [25].

TABLE I
RELATIVE DEPTH CONDITIONS FOR DEEP, INTERMEDIATE AND SHALLOW WATER WAVES.

Relative Depth (h/L)	Type of water wave
h/L > 0.5	Deep
0.04 ≤ h/L ≤ 0.5	Intermediate
h/L < 0.04	Shallow

TABLE II
THE VARIOUS REGIONS FOR GIVEN WAVE STEEPNESS.

Wave Steepness (H/L)	Region
H/L > 0.141	Wave breaking
0.04 < H/L < 0.141	Stokes Theory
H/L < 0.04	Linear Wave Theory

Relative depth therefore defines the type of wave. Deep water waves tend to have circular velocity orbitals due to having equal horizontal and vertical velocity components which decay exponentially through the water depth. Intermediate water waves have circular velocity orbitals, which turn more elliptical as the vertical component decays to zero at the seabed yet the horizontal component decays at the same rate as before. Shallow water waves possess a constant horizontal velocity component throughout the water depth whereas the vertical velocity decays to zero at the seabed. For the work presented in this paper, the relative depth conditions that represent deep and intermediate water waves were applied. The work also used S2OT as the theory is valid for waves with a greater steepness than LWT giving a bigger range of wave cases to test.

Regular waves travelling in the same direction as a uniform current will have a wave period (T_r), angular frequency (ω_r) and wave celerity (C_r) in a frame of reference that is moving at the same velocity as the current ($\overline{W}$) [25] [eq. (1)-(2)].

$$C_r = \frac{L}{T_r} \tag{1}$$

$$\omega_r = \frac{2\pi}{T_r} \tag{2}$$

In a stationary frame of reference, the waves will have a wave period (T_a), angular frequency (ω_a) and wave celerity (C_a). These parameters are calculated as follows [14] [eq. (3)-(5)]:

$$\frac{1}{T_a} = \frac{1}{T_r} + \frac{\overline{W}}{L} \tag{3}$$

$$C_a = C_r + \overline{W} \tag{4}$$

$$L = \frac{2\pi}{k} \tag{5}$$

Other important parameters include the wavelength (L), wave number (k), wave height (H) and water depth (h). The wave number can be calculated from eq. (6) which is known as the Dispersion Relation [26].

$$\omega_r{}^2 = gk\, tanh(kh) \tag{6}$$

When surface waves are superimposed on a uniform current, there is an interaction between these two components. The effect of the current causes the angular frequency of the waves (ω_r) to change due to the Doppler shift [11]. This change can be observed in eq. (7).

$$\omega_r = \omega_a - k \cdot \overline{W} \tag{7}$$

The surface elevation (η) of the wave is given by S2OT in eq. (8) [26]:

$$\eta = a\cos(kz - \omega_a t) + \frac{\pi H^2}{L}\frac{\cosh kh}{sinh^3 kh}(2 + \cosh 2kh)\, cos2(kz - \omega_a t) \tag{8}$$

where the amplitude (a) of the wave is $\frac{H}{2}$.

Surface gravity waves induce orbital motions in the horizontal (w_a) and vertical (v_a) direction to the path of wave propagation. These sub surface oscillations can penetrate the water column by up to half the wave length [14], and can be calculated in a stationary frame of reference using eq. (9)-(10) [26].

$$w_a = \overline{W} + a\omega_r \frac{\cosh k(h+y)}{\sinh(kh)}\cos(kz - \omega_a t) + \frac{3}{4}\left[\frac{\pi H}{L}\right]^2 C_r \frac{\cosh 2k(h+y)}{\sinh^4(kh)}\cos(2kz - 2\omega_a t) \tag{9}$$

$$v_a = a\omega_r \frac{\sinh k(h+y)}{\sinh(kh)}\sin(kz - \omega_a t) + \frac{3}{4}\left[\frac{\pi H}{L}\right]^2 C_r \frac{\sinh 2k(h+y)}{\sinh^4(kh)}\sin(2kz - 2\omega_a t) \tag{10}$$

III. NUMERICAL METHODOLOGY

The NWT used in this study was set up to replicate the University of Liverpool's recirculating water channel to enable a direct comparison between numerical and experimental results. The model dimensions were optimised for each simulation and were dependent upon the wave characteristic and water depth of the facility. The geometry and mesh were created using ANSYS ICEM 18.0 [27] while the physics setup, solver and results were all produced using ANSYS CFX 18.0 [28]. The model development has been split up into 3 main sections: *A. Geometry*, *B. Mesh* and *C. Physics Setup*.

A. Geometry

The working section of the University of Liverpool's recirculating water channel is 1.4m wide, 0.76m deep and 3.7m long [21] but the NWT was adapted for computational reasons to have a width of 0.1m, height of 1.09m and length of 20m. The width of the domain was limited to 0.1m to reduce the size of the model and therefore the computational effort needed to run the model without having an effect on the wave characteristics. The height of the NWT was calculated to have the SWL (0.76m) at 70% of the overall height which was recommended by [20]. This meant that the overall height was 1.09m to allow for a water depth of 0.76m with 0.33m at the top of the tank for an air space enabling a multiphase flow model to be used which will be discussed in Section C. The length of the NWT was extended to 20m to allow for 8-10 waves to propagate before reaching the end of the model as well as enabling a numerical beach of twice the wavelength (2L) to be incorporated as recommended by [29]. These settings meant that a region between 4-8m (2-4L) from the domain inlet possessed the desired wave-current characteristics.

B. Mesh

The mesh was developed using a ‘top down blocking strategy’ to create a HEXA mesh. 6 different HEXA meshes were created for a mesh independence study to ensure the mesh was refined to an acceptable level without compromising accuracy or being too computationally expensive.

1) Mesh Independence Study

Mesh optimisation is particularly important for free surface modelling, to enhance results and reduce computational effort. When modelling a NWT, there must be an increased mesh resolution at the fluid interface. This region must capture the entire wave height to maintain the desired surface resolution at all points along the wavelength. The meshing methods used are specified in terms of cells over the wave height and cells per wavelength so that they can be adapted for different wave cases.

It is recommend by [29] to use at least 10 cells over the height of the wave and at least 100 cells over the length of a single wave which agrees with the findings of [30]. It is suggested by [20] that an element size of 1/10th of the wave height is sufficient, while [31] states that 16 cells per wave height and 100 cells per wavelength produce mesh independent results. A summary of these results are shown in TABLE III.

TABLE III
RECOMMENDED MESH SETTINGS FOR FREE SURFACE MODELLING.

Author	**Cells over wave height (H)**	**Cells per wavelength (L)**
[20]	10	-
[29]	10-20	>100
[30]	10	145
[31]	16	100

TABLE IV shows the settings used in comparing 6 different meshing techniques based upon the findings of [20], [29]–[31]. It is important to note that only HEXA meshing was investigated in this mesh independence study. This is because less computational points are needed than a tetrahedral mesh, giving a higher spatial resolution with a better mesh aspect ratio increasing the accuracy of the simulation [31]. It also allows refinement of the mesh in the direction normal to the free surface without causing distortion in the other directions.

Figure 3 shows the normalised horizontal and vertical velocities at various points through a water depth of 0.76 m for a wave, superimposed on a current, with the following properties: T = 1.218s, H = 0.058m, $\overline{W}$ = 0.93m/s. Meshes 4 & 6 showed the closest agreement with the theoretical results produced using S2OT. However, as shown in Figure 4, mesh 6 is computationally much more expensive than mesh 4 which led to the selection of mesh 4, agreeing with the findings shown in TABLE III. Figure 2 shows the final mesh selection.

TABLE IV
A SUMMARY OF THE DIFFERENT MESH SET-UPS.

Mesh Number	**Cells over wave height (H)**	**Cells per wavelength (L)**	**Total Elements (thousands)**
1	10	60	378
2	10	80	488
3	10	100	620
4	10	120	730
5	10	140	839
6	20	100	1140

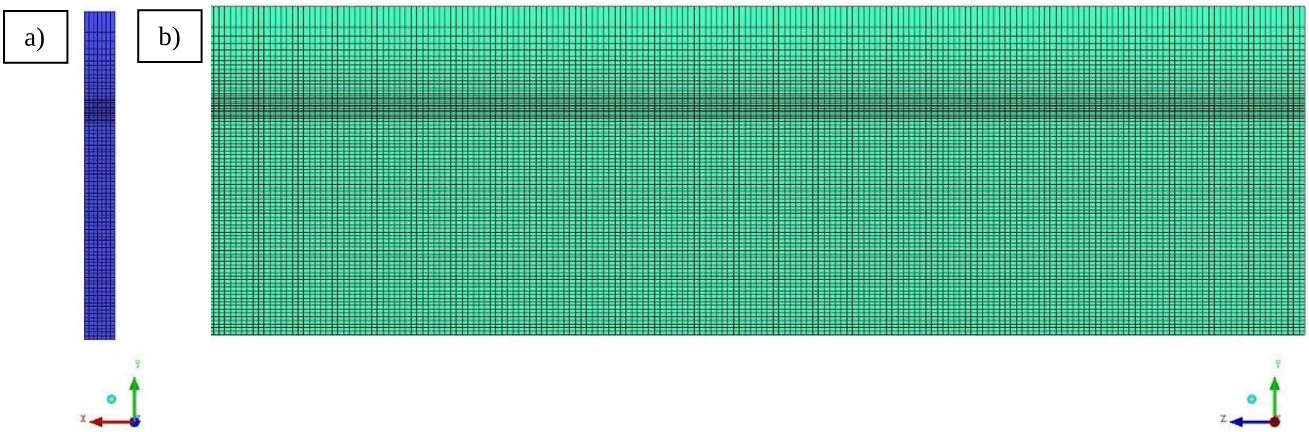

Figure 2. Final mesh selection using 120 cells per wavelength and 10 cells over the wave height: (a) in the XY plane and (b) in the YZ plane.

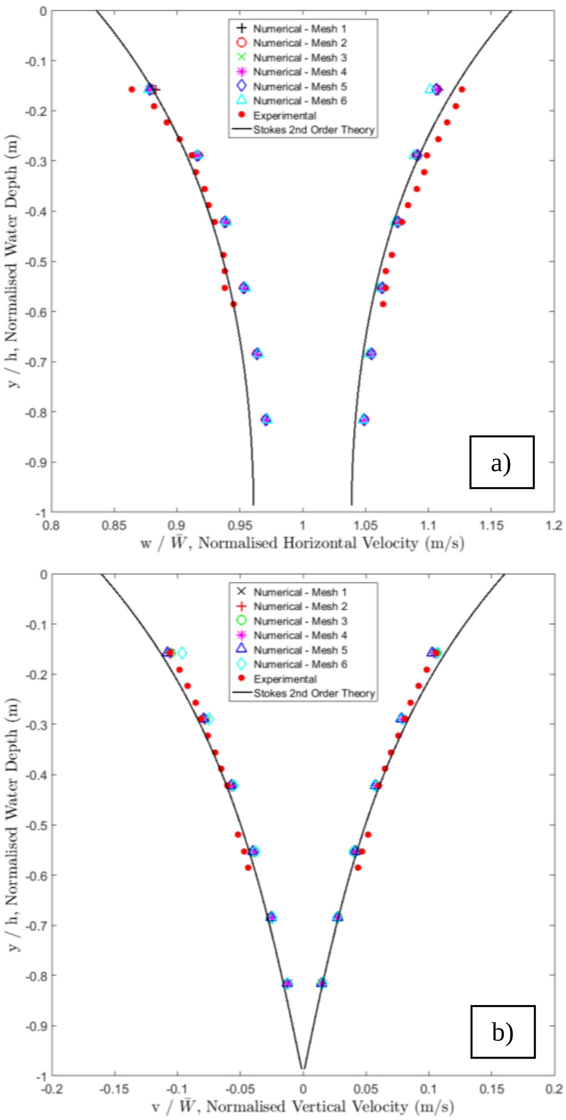

Figure 3. Normalised results for the numerical, theoretical and experimental maximum and minimum wave-induced: (a) horizontal velocities and (b) vertical velocities.

2) Time Step Study

A time step study was also carried out to look at the effect it had on computational effort and accuracy. The time step was specified in terms of the wave period and by dividing this into a certain amount of divisions, eg. T/50. Figure 5 shows that the smaller the time step used, the closer the numerical results are to the theoretical. However, as shown in Figure 6, the smaller the time step used, the more computationally expensive the model is. There was a considerable increase in accuracy between T/30 and T/50. However, above 50 divisions the results show little difference in accuracy yet a sizeable increase in computational run time. Hence, a time step of 50 divisions per wave period was chosen (T/50). This agrees closely with the findings of [30] who used a time step size of T/100, [32] who found T/40 was the maximum time step that could be used before numerical instability occurred, and [20] who stated that the optimum time step interval was T/50.

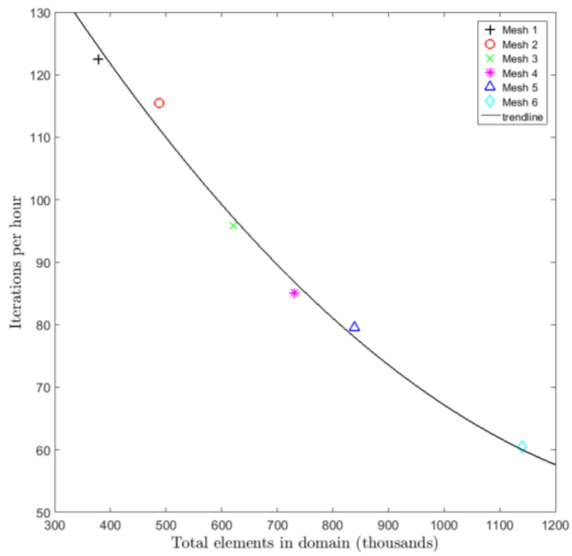

Figure 4. Computational speed of numerical model with different mesh sizes.

C. Physics Setup

ANSYS CFX 18.0 uses the Finite Volume Method (FVM) to discretise and solve the governing equations iteratively for small sub-divisions of the region of interest. This gives an approximation of each variable at points throughout the domain and so a picture of the full flow characteristic can be obtained [33]. The analysis is set up as a transient run using the time step found previously, 50 division per wave period (T/50). The Shear Stress Transport (SST) turbulence model is recommended for accurate boundary layer simulations [34] necessary in general turbine modelling. It has been applied in this study with foresight to investigate the wave-current interaction with one or more TSTs.

The following assumptions were made when defining the domain:

1. The air is defined as 25˚C with a density of 1.185 kg/m³
2. The water is defined as 25 ˚C with a density of 997 kg/ m³
3. The surface tension at the air-water interface is negligible
4. There is an initial hydrostatic pressure in the 'water' region and an atmospheric pressure in the 'air' region with this region being initially static
5. The seabed is horizontal and impermeable

The boundary conditions for this model were set as shown in Figure 7. The inlet was set as an 'opening' to allow flow into and out of the domain. This is necessary to prevent the model crashing as the horizontal and vertical velocities specified by S2OT for the wave at the inlet can produce back flow. The wave and current velocities were input using CFX Expression Language (CEL) [33] and were defined using volume fractions to differentiate between the 'water' and 'air' regions. The outlet was also set as an 'opening' to allow bidirectional flow. A hydrostatic pressure was used over the water depth up to the SWL as defined in Figure 1. The top of the domain was specified as an 'opening' with the air at atmospheric pressure. The two adjacent side walls were set as 'free-slip wall' so that shear stress at the wall is zero and the velocity of the fluid near the wall is not slowed by frictional effects. The base of the NWT was specified as 'no-slip' to model the frictional effects felt at the base of the tank. A summary of these boundary conditions are shown in TABLE V.

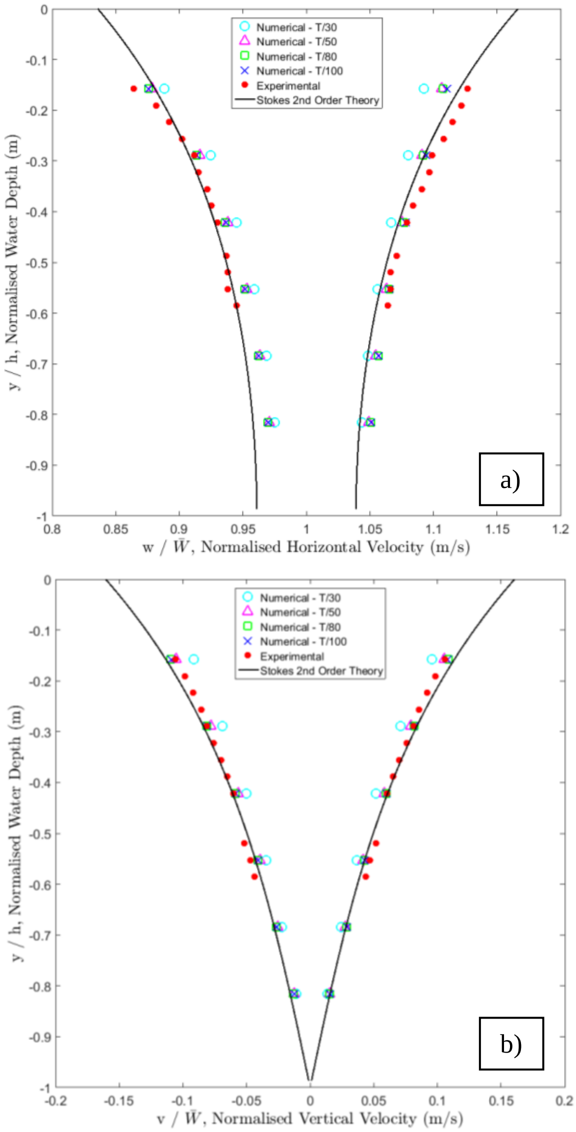

Figure 5. Normalised results for the numerical, theoretical and experimental maximum and minimum wave-induced: (a) horizontal and (b) vertical velocities for different time steps.

TABLE V
BOUNDARY CONDITION DETAILS.

Boundary	Boundary Condition
inlet	Velocity-inlet (opening)
outlet	Pressure-outlet (opening)
top	Pressure-opening
base	No-slip wall
walls	Free-slip wall

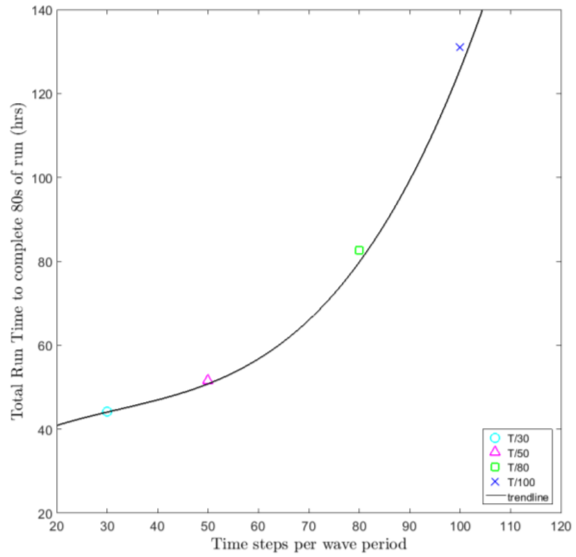

Figure 6. Computational speed of numerical model with different time steps.

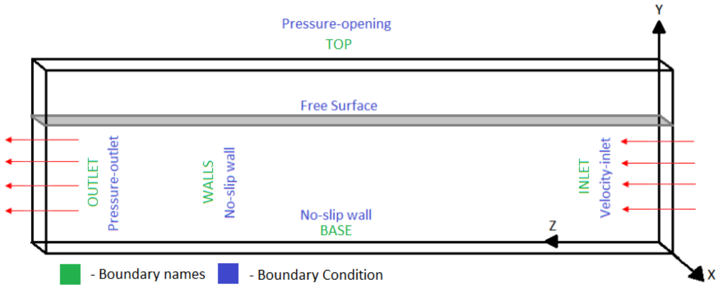

Figure 7. Boundary conditions for a 3D NWT.

A numerical beach was used to dampen out the waves and prevent any reflection from the end of the model. This was applied as a 'subdomain' over the whole model using CEL to target a distance 2L before the outlet. The mesh was also gradually increased in size, making it courser, in this region as recommended by [29]. The numerical beach was created by using a general momentum source acting in the stream wise direction. In this application, it was used to force the velocity in the beach region to be the same as the current velocity, removing the oscillatory effects of the wave. This was achieved by using eq. (11):

$$S_z = -C(U_z - U_{z,spec}) \tag{11}$$

Where S_z is the source term in the z-direction, $-C$ is the momentum source coefficient and should be set to a large number (eg. 10^5 kg/m³/s), U_z is the measured velocity at a certain point and $U_{z,spec}$ is the target velocity [33].

A homogenous multiphase model was used to model the free surface flow and is necessary when there is more than one fluid present. In this model, the 2 phases used were water and air. Volume fractions of each fluid are given by eq. (12):

$$V_1 = r_1 V \tag{12}$$

Where r_1 is the volume fraction of fluid 1, and V_1 is the volume occupied by fluid 1 in an overall volume, V [35]. 'Multiphase Control' is activated in the 'Solver Control' setup, using 'Segregated' for Volume Fraction Coupling and 'Volume-Weighted' for Initial Volume Fraction Smoothing.

The NWT was tested using the wave characteristics presented in TABLE VI. The tests were run so that each wave case was tested in 2 different water depths of h = 0.76m and h = 2.5m. Waves 1 & 2 are both classified as S2OT waves however Wave 3 is classified as a linear wave. Figure 8 shows the regions of validity and where each wave case sits when in an intermediate and deep water wave condition.

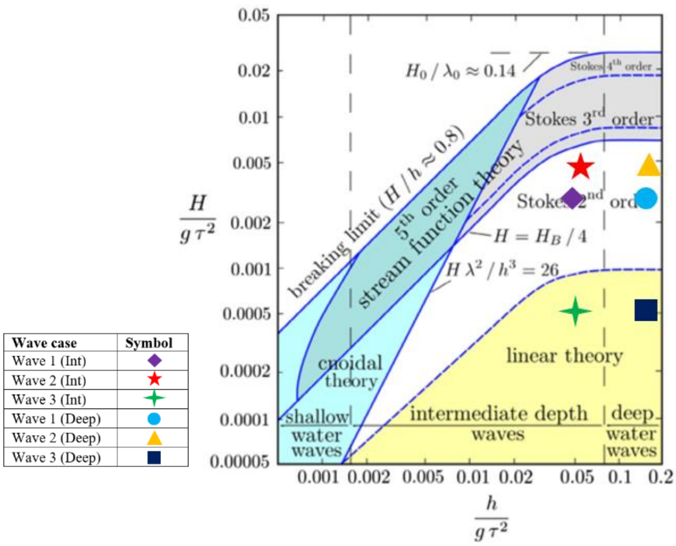

Figure 8. Regions of validity for each wave case in deep and intermediate water conditions [36].

Each test was initialised by having a uniform current velocity without the wave characteristic to allow the initial current flow to establish. After this, the wave case was superimposed onto the current and run for a total run time of over 100 seconds. Stability in the model occurred after 60 – 70 seconds and so all results reported in this study were taken over a 10 second period after 70 seconds of run time. Monitor points were added into the model in order to observe changes through the water depth in the velocity and wave period. The deep water cases were monitored at y = -0.1m, -0.3m, -0.5m, -0.7m, -0.9m, -1.1m, -1.3m & -1.5m, while the intermediate cases were monitored at y = -0.12m, -0.22m, -0.32m, -0.42m, -0.52m & -0.62m at various locations downstream of the inlet as shown in Figure 1.

These simulations all used 'Double Precision' when defining the run. This setting permits more accurate numerical mathematical operations and can improve convergence. It is recommended for all multiphase modelling [33]. This work was carried out using parallel processing, specifically 32 processors over 2 nodes, using the computational facilities of the Advanced Research Computing @ Cardiff (ARCCA) Division, Cardiff University.

IV. Results and Discussion

A. Deep Water Wave Conditions

The following results are for deep water wave cases, modelled with a water depth of h = 2.5m. Figure 9 shows that excellent agreement was found between the numerical and theoretical surface elevation for each wave case. The % error between the numerical and theoretical results for the surface elevation were 0.17%, 0.27% & 0.01% for Wave 1, 2 & 3 respectively. The average wave period (T_a) of the numerical models were 0.818s (W1), 0.755s (W2) & 1.155s (W3) which agreed exactly with the theoretical values input to the model.

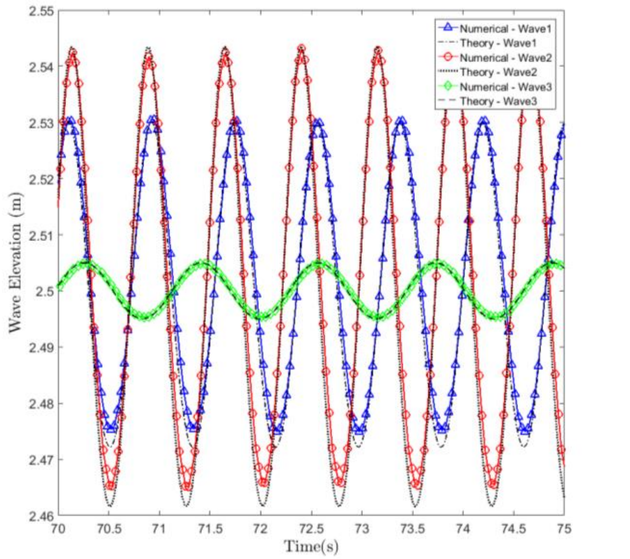

Figure 9. Surface elevation of Wave 1, 2 & 3 in deep water conditions at location 4m downstream of inlet.

Figure 10 shows the horizontal and vertical velocities through the water depth for the numerical and theoretical results. Both sets of numerical velocities showed a good agreement with the theory. For the horizontal velocities, Waves 1 & 3 always had a difference of less than 1.5% of the mean stream wise velocity while Wave 2 had a slightly greater difference of 3%. The vertical velocities showed better agreement with Waves 1 & 3 having a difference of less than

TABLE VI
WAVE CHARACTERISTICS USED.

Wave Name	H (m)	Tr (s)	L (m)	$\overline{W}$ (m/s)	H/L	h/L [h = 0.76m]	h/L [h = 2.5m]
Wave 1	0.058	1.218	2.25	0.93	0.026	0.338	1.11
Wave 2	0.082	1.147	2.02	0.93	0.041	0.376	1.24
Wave 3	0.01	1.218	2.25	0.1	0.004	0.338	1.11

1% of the mean stream wise velocity while Wave 2 had a difference of less than 1.5%. Both sets of results showed the biggest differences were towards the surface of the water where the oscillations were greater.

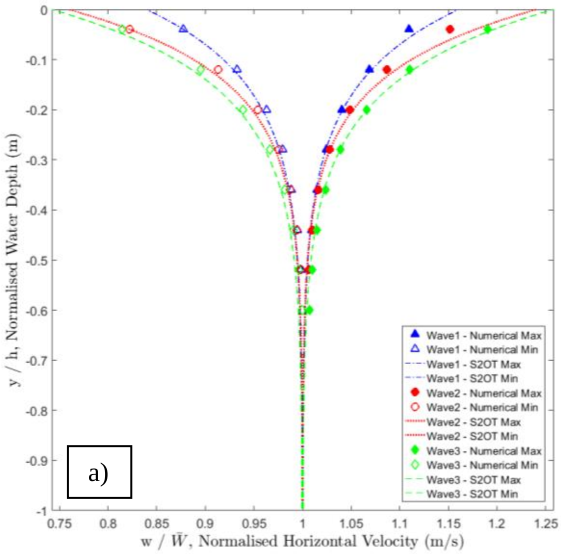

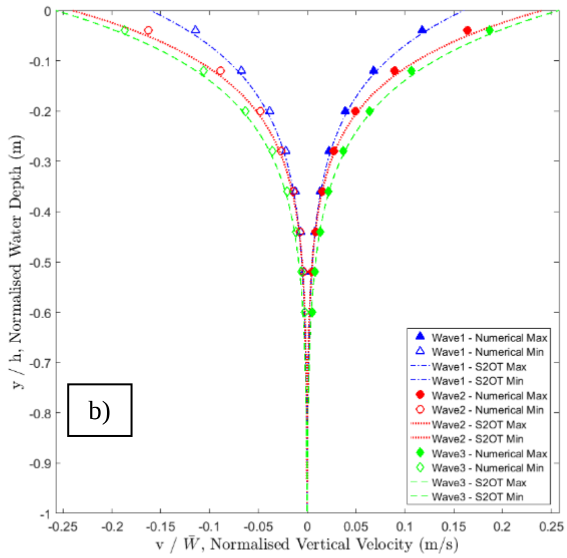

Figure 10. The normalised a) horizontal and b) vertical velocities at monitor points through the water depth at a location 4m downstream of the inlet for numerical results and S2OT.

Due to the relative depth (h/L) of these deep water wave cases, it can be seen that the velocity fluctuations are minimal half way down the water column, with oscillations decaying completely by the time they reach the bottom of the tank. Therefore, if a marine device was placed in the bottom half of the water depth it would encounter minimal velocity variations while still being able to extract energy from the dominating current flow. For certain deployment sites with devices positioned in an area of relatively uniform flow, this type of model could be used to gather information on the flow characteristics present in relatively steady flow regions. For other sites with highly sheared flow conditions a profiled flow model would be more appropriate [37].

B. *Intermediate Water Wave Conditions*

The following results are for intermediate water wave cases, modelled with a water depth of h = 0.76m. All wave cases were compared to theory but wave cases 1 & 2 could also be compared to experimental results obtained by the University of Liverpool. The experimental results obtained by the University of Liverpool were collected over 250 wave cycles and averaged to determine the mean wave profiles. It was found that the wave height could vary by ±5% and the wave period by ±0.5%. The vertical and horizontal velocities were measured using an Acoustic Doppler Velocimeter (ADV), which gave the results an uncertainty of ±1%. The ADV covered a depth range from y = -0.12m to y = -0.42m with y = 0m being at the SWL [21].

Figure 11 shows the numerical and theoretical surface elevation for each wave case at an intermediate depth. The % error between the numerical and theoretical surface elevation for Wave 1, 2 & 3 was 1.01%, 1.61% & 0.05% respectively. This is slightly bigger than the deep water surface elevation % errors but still at an acceptable level. The same % errors are apparent when compared to the experimental results as these average results are the same as the theory. The average wave period (T_a) of the numerical models was 0.81s (W1), 0.75s (W2) & 1.15s (W3) which again agreed precisely with the theoretical values input to the model. Again, the experimental results were the same as the theory and so these results also showed good agreement with the average wave period for each wave case.

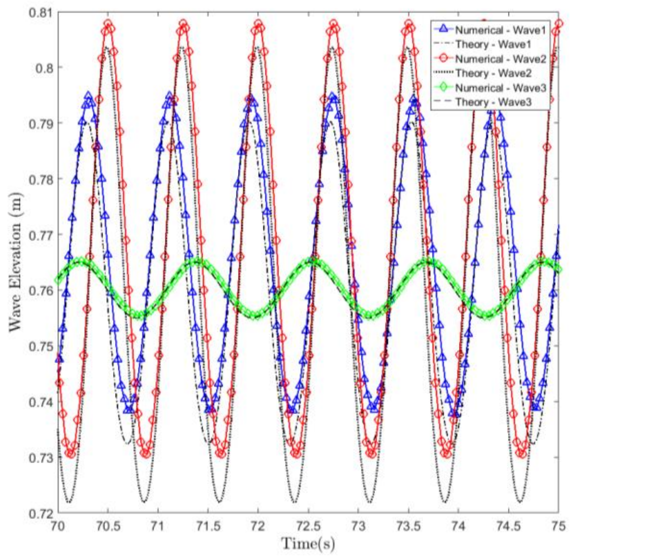

Figure 11. Surface elevation of Wave 1, 2 & 3 in intermediate water conditions at location 4m downstream of inlet.

The horizontal and vertical velocities given by the numerical model at points through the water depth are shown in Figure 12. In both cases the numerical velocities gave a good comparison to the theoretical results. For the horizontal velocities, the numerical results had a difference of less than 3% of the mean stream wise velocity, while for the vertical velocities the numerical results had a difference of less than 2%. When comparing the numerical against the experimental results, Wave 1 had a difference of less than 1% of the stream wise velocity and Wave 2 had a difference of less than 4%.

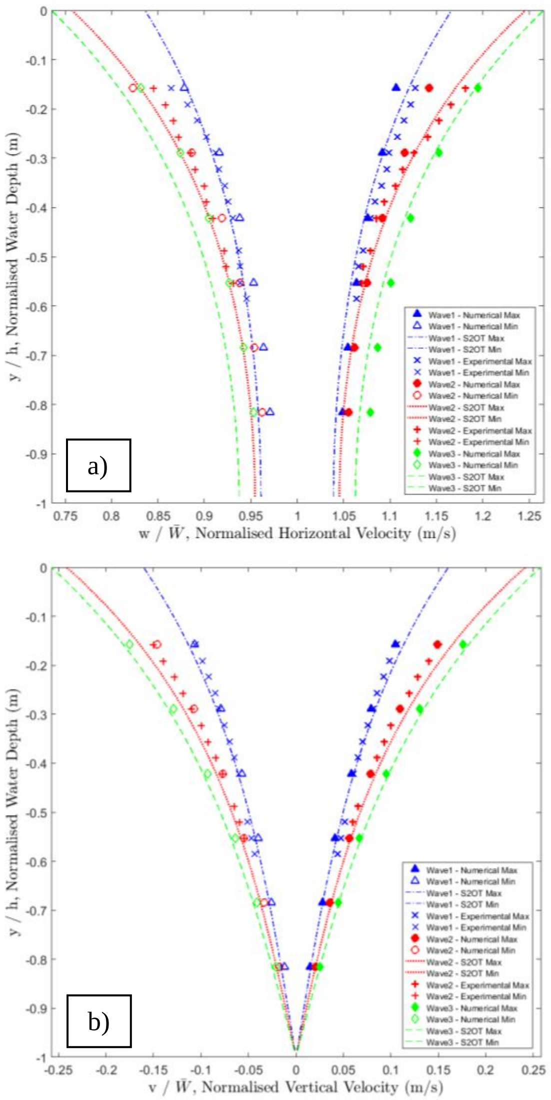

Figure 12. The normalised a) horizontal and b) vertical velocities at monitor points through the water depth at a location 4m downstream of the inlet for numerical results, experimental results and S2OT.

It was clear to see that the horizontal velocities of the intermediate water conditions still had a considerable oscillatory effect near the bottom of the tank in comparison to the vertical velocities, which tended to zero at the bottom of the tank. This causes the shape of the orbitals to be more circular near the surface of the water and become elliptical towards the bottom of the tank. This can be seen in Figure 13 where the normalised maximum and minimum, horizontal and vertical velocities have been plotted for Wave 1 to give an estimation of the orbital shapes and sizes through the water column. This is different to the deep water wave conditions where both the horizontal and vertical velocities tended to zero at the bottom of the tank. It can be seen from Figure 13 that the orbitals are much more circular for the deep water wave case than the intermediate water wave case. These results are what would be expected for deep and intermediate water wave conditions.

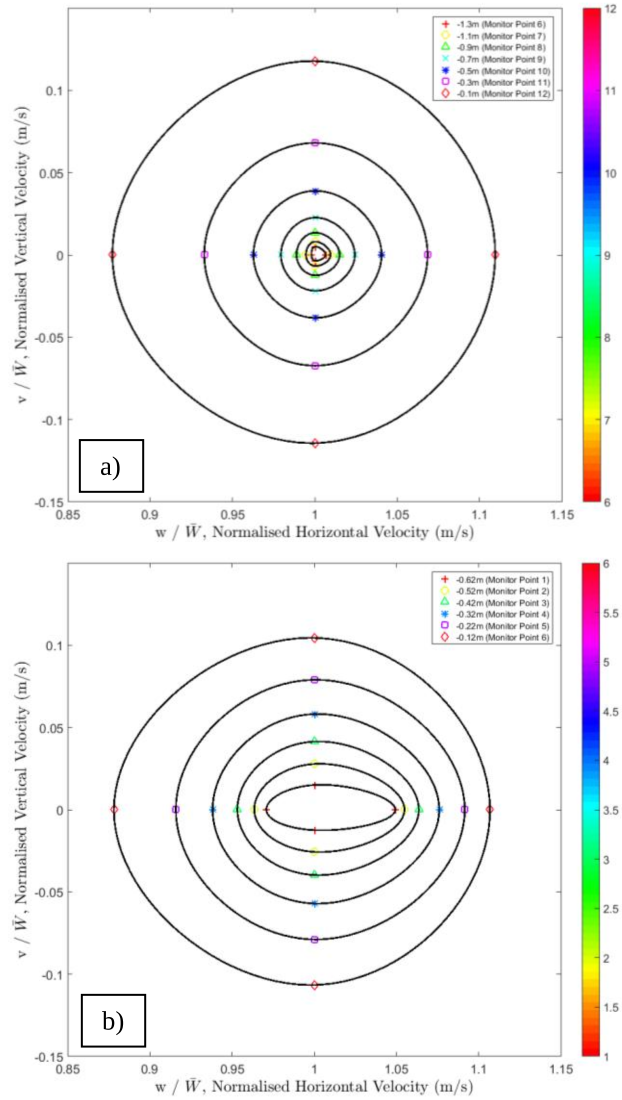

Figure 13. Normalised maximum and minimum, horizontal and vertical velocities to give an idea of the shape and magnitude of the velocity orbitals for a) deep and b) intermediate water wave conditions for Wave 1.

The mesh selection was extremely important in enabling the numerical model to have good agreement with the theoretical and experimental results. This study, however, only looked at using a HEXA mesh to create the NWT and other meshing techniques could be further investigated. Validation of this NWT has been achieved using S2OT and experimental results using 3 different wave cases in 2 different depth tanks. As shown in Figure 8, the 6 tests that were modelled over a broad area of theories as well as intermediate and deep water conditions. This model could be tested further by using Stokes 3rd, 4th or 5th Order Theories to test waves with larger amplitudes. Further work will build upon this set of guidelines for wave-current modelling and develop a profiled flow model giving a broader range of wave-current conditions that can be tested.

V. Conclusion

The aim of this study was to develop a NWT to simulate the wave-current interaction between regular waves and a uniform current velocity. 6 simulations were carried out using 3 different wave characteristics and 2 different depth tanks. The regular wave cases were all within the S2OT and linear wave regions. Guidelines for the development of an optimum NWT have been established, detailing the importance of mesh development and model setup. The optimum mesh size and time step was found to have 10 cells over the wave height and 120 cells per wavelength with a time step of T/50. The model was set up as a homogenous multiphase model using volume fractions to differentiate between phases and was developed using ANSYS ICEM 18.0 and ANSYS CFX 18.0. Numerical results for all 6 simulations were in good agreement with theoretical and experimental results. This study has shown that numerical models can effectively replicate ocean wave and current conditions presenting a cheaper alternative to physical model scale testing.

Acknowledgements

The authors acknowledge support from SuperGen UK Centre for Marine Energy (EPSRC: EP/N020782/1) and the University of Liverpool are thanked for providing experimental data. This work was carried out using the computational facilities of the Advanced Research Computing @ Cardiff (ARCCA) Division, Cardiff University. Authors are grateful to PRIMaRE for supporting the travel to this event through an Early Career Research Travel Grant (ECR-TG), which has received funding from EPSRC under grant agreement EP/P026109/1.

References

[1] U.S Energy Information Administration, "International Energy Outlook 2017," 2017.

[2] Ocean Energy Europe, "Ocean energy project spotlight: Investing in tidal and wave energy," 2017.

[3] EDF France, "Tidal Power." [Online]. Available: https://www.edf.fr/en/the-edf-group/industrial-provider/renewable-energies/marine-energy/tidal-power. [Accessed: 30-Jan-2018].

[4] Tidal Lagoon Plc and Tidal Lagoon (Swansea Bay) Plc, "Swansea Bay - Tidal Lagoon." [Online]. Available: http://www.tidallagoonpower.com/projects/swansea-bay/. [Accessed: 30-Jan-2018].

[5] Atlantis Resources, "Project Development and Operation - MeyGen." [Online]. Available: https://www.atlantisresourcesltd.com/projects/meygen/. [Accessed: 26-Jan-2018].

[6] EDF France, "Paimpol-bréhat Hydrolienne: the big dive." [Online]. Available: https://www.edf.fr/edf/accueil-magazine/hydrolienne-de-paimpol-brehat-le-grand-plongeon. [Accessed: 30-Jan-2018].

[7] E. Lust, L. Luznik, K. Flack, J. Walker, and M. Van Benthem, "The influence of surface gravity waves on marine current turbine performance," *Int. J. Mar. Energy*, vol. 3–4, pp. 27–40, 2013.

[8] L. Luznik, K. A. Flack, E. E. Lust, and K. Taylor, "The effect of surface waves on the performance characteristics of a model tidal turbine," *Renew. Energy*, vol. 58, pp. 108–114, 2013.

[9] M. Sos, L. Johnston, J. Walker, and M. Rahimian, "The impact of waves and immersion depth on HATT performance," *Proc. 12th Eur. Wave Tidal Energy Conf. 27th Aug -1st Sept 2017, Cork, Irel.*, pp. 1–8, 2017.

[10] N. Barltrop, K. S. Varyani, A. Grant, D. Clelland, and X. P. Pham, "Investigation into wave-current interactions in marine current turbines," *Proc. IMechE, Part A J. Power Energy*, vol. 221, no. 2, pp. 233–242, 2007.

[11] P. W. Galloway, L. E. Myers, and A. S. Bahaj, "Studies of a scale tidal turbine in close proximity to waves," *3rd Int. Conf. Ocean Energy, Bilbao, Spain, 6 Oct 2010*, no. 1, pp. 3–8, 2010.

[12] B. Gaurier, P. Davies, A. Deuff, and G. Germain, "Flume tank characterization of marine current turbine blade behaviour under current and wave loading," vol. 59, pp. 1–12, 2013.

[13] Tidal Stream Ltd, "Resource," 2016. [Online]. Available: http://www.tidalstream.co.uk/Resource/resource.html. [Accessed: 12-Dec-2017].

[14] R. Sorensen, *Basic Coastal Engineering*, 3rd ed. Pensylvania: John Wiley & Sons, 2006.

[15] X.-F. Liang, J.-M. Yang, J. Li, X. Long-Fei, and L. Xin, "Numerical Simulation of Irregular Wave - Simulating Irregular Wave Train," *J. Hydrodyn.*, vol. 22, no. 4, pp. 537–545, 2010.

[16] S. F. Sufian, M. Li, and B. A. O'Connor, "3D Modeling of Impacts from Waves on Tidal Turbine Wake Characteristics and Energy Output," *Renew. Energy*, pp. 1–15, 2017.

[17] X. Tian, Q. Wang, G. Liu, W. Deng, and Z. Gao, "Numerical and experimental studies on a three-dimensional numerical wave tank," *IEEE Access*, vol. 3536, no. c, pp. 1–1, 2018.

[18] A. Lal and M. Elangovan, "CFD Simulation and Validation of Flap Type Wave-Maker," *Int. J. Math. Comput. Sci.*, vol. 2, no. 10, pp. 708–714, 2008.

[19] S. C. Tatum *et al.*, "Wave-current interaction effects on tidal stream turbine performance and loading characteristics," *Int. J. Mar. Energy*, vol. 14, pp. 161–179, 2016.

[20] W. Finnegan and J. Goggins, "Numerical simulation of linear water waves and wave–structure interaction," *Ocean Eng.*, vol. 43, pp. 23–31, 2012.

[21] T. D. J. Henriques, T. S. Hedges, I. Owen, and R. J. Poole, "The influence of blade pitch angle on the performance of a model horizontal axis tidal stream turbine operating under wave-current interaction," *Energy*, vol. 102, pp. 166–175, 2016.

[22] G. B. Airy, "Tides and Waves," *Encycl. Metrop.*, vol. 5, pp. 341–396, 1845.

[23] V. Sundar, *Ocean Wave Mechanics: Applications in Marine Structures*. London: Wiley, 2016.

[24] G. G. Stokes, "On the theory of oscillatory waves," *Trans. Cambridge Philos. Soc.*, vol. 8, pp. 441–455, 1847.

[25] T. S. Hedges, "Regions of validity of analytical wave theories," *Proc. Inst. Civ. Eng. - Water Marit. Eng.*, vol. 112, no. 2, pp. 111–114, 1995.

[26] J. S. Mani, *Coastal Hydrodynamics*. New Delhi: PHI Learning Private Limited, 2012.

[27] ANSYS Inc, "ANSYS ICEM." Release 18.0.

[28] ANSYS Inc, "ANSYS CFX." Release 18.0.

[29] ANSYS Inc., "ANSYS Fluent Advanced Workshop: Simulation of Small Floating Objects in Wavy Environment with ANSYS Fluent," 2016.

[30] M. C. Silva, M. A. Vitola, P. T. T. Esperanca, S. H. Sphaier, and C. A. Levi, "Numerical simulations of wave-current flow in an ocean basin," *Appl. Ocean Res.*, vol. 61, pp. 32–41, 2016.

[31] A. Raval, "Numerical Simulation of Water Waves using Navier-Stokes Equations," University of Leeds, 2008.

[32] D. Ning and B. Teng, "Numerical simulation of fully nonlinear irregular wave tank in three dimension," *Int. J. Numer. Methods Fluids*, no. November 2006, pp. 1847–1862, 2007.

[33] ANSYS Inc, "ANSYS CFX Modelling Guide." Release 18.0, Help System.

[34] ANSYS Inc, "Innovative Turbulence Modeling: SST Model in ANSYS CFX," 2004.

[35] ANSYS Inc, "ANSYS CFX Theory Guide." Release 18.0, Help System.

[36] B. Le Mehaute, *An Introduction to Hydrodynamics and Water Waves*. New York: Springer-Verlag, 1976.

[37] T. O'Doherty, A. Mason-Jones, D. O'Doherty, P. Evans, C. Wooldridge, and I. Fryett, "Considerations of a horizontal axis tidal turbine," *Proc. Inst. Civ. Eng. - Energy*, vol. 163, no. EN3, pp. 119–130, 2010.